# Nb-H system at high pressures and temperatures

Guangtao Liu,[1,2,6] Stanislav Besedin,[2] Alla Irodova,[3] Hanyu Liu,[4] Guoying Gao,[5] Mikhail Eremets,[2] Xin Wang,[1] and Yanming Ma[1,7,*]

[1]*State Key Laboratory of Superhard Materials, Department of Physics, Jilin University, Changchun 130012, China*

[2]*Max Planck Institute for Chemistry, Mainz 55020, Germany*

[3]*National Research Centre "Kurchatov Institute," Moscow, Russia*

[4]*Geophysical Laboratory, Carnegie Institution of Washington, Washington, DC 20015, USA*

[5]*State Key Laboratory of Metastable Materials Science and Technology, Yanshan University, Qinhuangdao 066004, China*

[6]*National Key Laboratory of Shock Wave and Detonation Physics, Institute of Fluid Physics, China Academy of Engineering Physics, Mianyang 621900, China*

[7]*International Center of Future Science, Jilin University, Changchun 130012, China*

(Received 9 December 2016; published 24 March 2017)

We studied the Nb-H system over extended pressure and temperature ranges to establish the highest level of hydrogen abundance we could achieve from the resulting alloy. We probed the Nb-H system with laser heating and x-ray diffraction complemented by numerical density functional theory-based simulations. New quenched double hexagonal close-packed (hcp) $NbH_{2.5}$ appears under 46 GPa, and above 56 GPa cubic $NbH_3$ is formed as theoretically predicted. Nb atoms are arranged in close-packed lattices which are martensitically transformed in the sequence: face-centered cubic (fcc) → hcp → double hcp (dhcp) → distorted body-centered cubic (bcc) as pressure increases. The appearance of fcc $NbH_{2.5-3}$ and dhcp $NbH_{2.5}$ cannot be understood in terms of enthalpic stability, but can be rationalized when finite temperatures are taken into account. The structural and compressional behavior of $NbH_{x>2}$ is similar to that of NbH. Nevertheless, a direct H-H interaction emerges with hydrogen concentration increases, which manifests itself via a reduction in the lattice expansion induced by hydrogen dissolution.

DOI: 10.1103/PhysRevB.95.104110

## I. INTRODUCTION

To date, very few of the stable metal polyhydride predictions have been fully examined or confirmed due to current experimental limitations. Here, we studied the Nb-H system both experimentally and theoretically up to 1 megabar. Using diamond anvil cell (DAC), laser heating and *in situ* synchrotron x-ray diffraction (XRD), we successfully synthesized and measured several new phases of $NbH_x$. $NbH_{2-2.5}$ underwent a phase transition from a face-centered-cubic (fcc) phase to an irregular hexagonal phase at 39 GPa. Interestingly, we observed hexagonal-close-packed (hcp)/double-hcp (dhcp) $NbH_{2.5}$ and distorted body-centered-cubic (bcc) $NbH_3$ above 56 GPa along a different thermodynamic path, which was supported by our first principles calculations. Our findings provide insights into the formation of metal polyhydrides at extreme conditions, which may have energy storage potential in the future.

Transition metal hydrides have been studied for many decades to address a broad range of applied and fundamental problems [1–3]. Nowadays, the emphasis has shifted towards compounds with a high hydrogen content, due to the increasing demand for hydrogen storage materials for mobile applications [4,5] and the suggestion that hydrogen-dominated metallic alloys may be high temperature superconductors [6]. The recent discovery of superconducting behavior in sulfur hydride with a record critical temperature ($T_c$) of 203 K at 155 GPa [7] has added even more intrigue to this issue, which is inspired by a theoretical prediction [8]. It is speculated that metallic hydrogen could also be a high-$T_c$ superconductor [9], but its metallization pressure is still experimentally unreachable. Combining hydrogen with another appropriate element gives rise to "chemical precompression", where a metallic state may be reached at lower pressures. There are three essential chemical precompression mechanisms (see also Ref. [10] for more details about role of impurity in dense hydrogen): (i) First, it appears when a covalent bond between hydrogen and the admixing element is formed. The latter contributes its electrons into common electronic band(s), thus increasing valence electron density. According to the Goldman-Herzfeld criterion, this acts in the same way as external pressure towards turning material to a metallic state. In particular, this should happen in the group IVA element hydrides [6]. (ii) Second, hydrogen remains in a molecular state, but the $H_2$ molecule is impelled towards dissociation under compression, due to the partial occupation of its antibonding states by the electrons from the dopant atom. This mechanism is suggested to be in action when some of the metals are added to hydrogen, such as the Li-H [11], Na-H [12], Ca-H [13], and Y-H [14] systems. (iii) The third mechanism results from the previous one: once the electrons have been transferred to $H_2$, both the admixing element and the hydrogen molecule become charged. The Madelung forces then act by compressing the system. The Madelung precompression is effective at low pressures, when repulsion by the core electrons does not overwhelm effect of electrostatic interaction. In particular, it has pronounced effect in the Li-H [11] and Na-H [12] systems.

Whether or not a precompressed system will be a superconductor depends on the particular dopant. Many systems have been examined theoretically, and a few $T_c$ were predicted to be even higher than in sulfur hydride, such as $T_c = 220$ K at 150 GPa for $CaH_6$ [13], $T_c = 250$ K at 110 GPa for $YH_6$ [14], and $T_c = 260$ K at 300 GPa for $MgH_6$ [15]. According to

*Corresponding author: mym@jlu.edu.cn

 

calculations, these systems become enthalpically stable with respect to their pure constituents at corresponding pressures. In practice, incorporating the necessary dopants appeared to be not a trivial problem, but none of the systems mentioned have been synthesized experimentally so far. Examining other typical systems with this background knowledge is beneficial because, even if their $T_c$ are not very high or they have no superconductivity at all, systematic studies can shed light on the properties of the admixing element(s) as well as the features of the resulting hydrides which can give rise to superconductivity.

When the $H_2$ molecule is absorbed on the surface of a transition metal, it breaks down, and the H atoms migrate into the metal forming a metal-hydrogen alloy. This process can be viewed as the "ultimate" case of chemical precompression in the sense of the second mechanism: here, complete dissociation of the hydrogen molecule takes place. Although hydrogen is placed into a metallic environment, in fact it has little in common with metallic hydrogen because the electronic properties of hydride are mainly determined by the narrow $d$ bands of their host metal [16]. This is, at least partially, a consequence of the low hydrogen content, where hydrogen acts as the dopant element. It is obvious that an increase of the hydrogen concentration will eventually make the alloy hydrogen dominant. Thus, in which way does the resulting hydride adopt features and characteristics of precompressed hydrogen, and in what composition does it happen? For transition metal hydride, theoretical studies of the W-H [17] and Nb-H [18] systems suggest that several stoichiometries $MeH_x$ ($Me$ = Nb, W) could be enthalpically stable at high pressures with $x$ varying up to 6 for Nb and 8 for W. The hydrogen sublattice forms a three-dimensional (3D) network without H-H pairing, but its structure cannot be described as possessing some characteristic features, for example, the sodalite cages in the Ca-H and Y-H systems. Experimentally, $RhH_2$ was discovered at 8 GPa first [19]. The W-H system was studied up to 100 GPa and above 1000 K [17,20]. The $WH_x$ alloy formed at pressures above 25 [20] or 30 [17] GPa with its maximum hydrogen content reaching $x = 4/3$ [20], while $IrH_3$ [21] and $FeH_3$ [22] were synthesized under extreme conditions.

Here, we address the issue of hydrogen solubility in transition metals by studying the Nb-H system. We chose this system, first, to examine whether an alloy $NbH_{x>2}$ can be synthesized when pressure is varied up to 100 GPa as theoretically predicted [18] and, second, because the Nb-H system has been studied thoroughly in the past, both experimentally and theoretically, which enables us to trace the evolution of the hydrogen state in transition metals up to an as yet unexplored hydrogen concentration range.

## II. HYDROGEN IN NIOBIUM: SOME BASIC PROPERTIES

When hydrogen dissolution occurs at elevated temperatures up to 1000 K and pressures ranging from $10^{-6}$ to $10^2$ bar, H atoms randomly occupy the tetrahedral (T) interstices of the host metal, resulting in the formation of a $NbH_x$ alloy, whose hydrogen contents vary in the interval of $0.01 < x < 1.1$ as a function of pressure and temperature [1]. The lattice parameter of the hydride is larger than that of pure Nb, and the expansion amounts to $\sim 2.9\,\text{Å}^3$/H atom [23]. This value also holds for many other hydrides and is often used to evaluate their hydrogen concentration when other methods are not available, particularly in DAC experiments. The Nb-H system phase diagram appears to be quite complicated [1] and has a few features which are relevant to this paper. First, it is important to distinguish between the two phases that correspond to the bcc Nb lattice with disordered hydrogen: the $\alpha$ phase with lower hydrogen content and the $\alpha'$ phase with a higher concentration because there is a region of the phase diagram ($0.1 < x < 0.5, 360 < T < 450$ K) where two bcc lattices with different lattice parameters coexist. This phenomenon is called spinodal decomposition into coherent and noncoherent phases [3] or alternatively phase transition from lattice gas to lattice liquid in the hydrogen subsystem [2]. At lower temperatures (below 360 K) and higher hydrogen content ($x > 0.7$), there are several phases where hydrogen is interstitially ordered [2]. This hydrogen ordering causes lattice distortion of the host metal. In particular, the structure of the $\beta$ phase is base-centered orthorhombic. As pressure is increased to a few bars and above room temperature, the $\gamma$ phase appears which is essentially stoichiometric $NbH_2$ [24]. The host lattice changes from bcc to fcc where all hydrogen occupy the T interstices and no single phase is known with a hydrogen content of $1 < x < 2$.

## III. METHODS

### A. Experiments

Pressure was generated using the DAC technique. For pressures in the 0–50 GPa interval, flat anvils were used with culets diameter of 220 $\mu$m in cell 1. For higher pressures, single beveled diamonds were used with culets size of 100 $\mu$m (bevel angle is 7.5° and total tip size is 300 $\mu$m) in cell 2. We used gaskets made of a mixture of epoxy with cubic BN. The thicknesses of gaskets were about 20 and 10 $\mu$m for the flat and beveled anvils accordingly. A neodymium-doped yttrium aluminum garnet (Nd:YAG) laser in the multimode regime was used to heat the sample from a single side, and pressure was measured by both using the diamond-edge scale [25] and pressure dependence of hydrogen vibron [26].

We compressed a commercial 3 $\mu$m thick Nb foil of 99.9% purity (Goodfellow) between two anvils to obtain a $\sim$1 $\mu$m thick Nb foil and used a chip of this as our sample. Both sides of the sample were subjected to ion etching to remove the surface oxide layer and covered with $\sim$20 nm thick Pd film using the magnetron sputter method to protect them from oxidization again. The Pd films also served as a membrane to facilitate the hydrogen penetration of the sample [27]. For laser heating, a flake of hexagonal BN was placed between the Nb foil and one of the culets to thermally insulate the sample from the diamond. All culets were covered with a $\sim$20 nm MgO film to protect the diamond from hot $H_2$. Here, $H_2$ of 99.999% purity (Air Liquid) was loaded into the DAC at room temperature under $\sim$1500 bar.

X-ray diffraction measurements were mainly performed at beamline I15 of the Diamond Light Source, but a portion of the measurements were performed at beamline P02.2. of the PETRA III Synchrotron Source. At beamline I15, the incident beam was focused to 70 $\mu$m and then collimated to 20 $\mu$m in

diameter. The sample detector distance and geometric parameters were calibrated using standard silicon. Powder diffraction data was collected using two-dimensional (2D) Mar 345 Image Plate Detector (PerkinElmer Detector was used at P02.2.) and the typical exposure time was 20–60 s. Here, FIT2D software was used to convert the 2D data to one-dimensional (1D) diffraction profiles, which were then analyzed using the FullProf software suite [28] for structure solution.

### B. Calculations

For extra data analysis and interpretation, density functional theory (DFT) calculations were mainly performed with Vienna *Ab initio* Simulation Package (VASP) [29] and Quantum Espresso (QE) [30] codes. The Perdew-Burke-Ernzerhof (PBE) exchange-correlation functional was used in the calculations. In the calculations with VASP, the all electron projector augmented wave method was used. Part of the QE calculations were made using the Rappe-Rabe-Kaxiras-Joannopoulos (RRKJ) pseudopotential and another part using the all electron Electrons in k-space (ELK) method [31]. In the calculations with VASP, the $4s^2 4p^6 4d^4 5s^1$ and $1s^1$ electrons were treated as valence electrons for Nb and H, respectively. To ensure that all enthalpy calculations were well converged to less than 1 meV/atom, the Monkhorst-Pack grid with sufficient density ($2\pi \times 0.025$ Å$^{-1}$) in reciprocal space as well as appropriate cutoff energy (600 eV) were chosen. The Crystal Structure Analysis by Particle Swarm Optimization (CALYPSO) code [32,33] was employed for crystal structure search, which is based on a global minimum of search of free energy surfaces calculated by the DFT total energy calculations through the particle swarm optimization algorithm. The simulation cell comprised of 1 to 8 formula units at 30, 50, and 80 GPa. The phonon calculations were carried out using a finite displacement approach [34] through the PHONOPY code [35], which uses the Hellmann-Feynman forces calculated from the optimized supercell through VASP.

## IV. RESULTS

### A. Compression at room temperature

In the first run, XRD measurements were performed from 22 to 119 GPa. This compression run started 2 d after the sample was loaded into the DAC and lasted for several hours. No other peak than the one belonging to the bcc Nb lattice was observed. Then, after about 36 hours, another x-ray exposure was taken at 119 GPa, as shown in the Fig. S1 in the Supplemental Material [36]. Two new weak peaks appeared to the left from the strongest leftmost bcc peak (Nb-110) indicating that a small amount of hydride may have formed. This also indicates slow kinetics of hydride formation.

For the second run, two cells were loaded 1 wk before the XRD measurements. The XRD measurement of the bcc pattern splitting was observed immediately in both cells and remained up to the highest pressures reached: 56 GPa with cell 1 and 110 GPa with cell 2 (Fig. S2 in the Supplemental Material [36]). Unit cell volumes were obtained from the higher-angle sets of peaks when plotted versus pressure coincide with the equation of state (EOS) for Nb. The lower-angle set is therefore attributed to the hydride $NbH_x$. From the volume difference between Nb and $NbH_x$, the hydrogen content is obtained as $x = 0.5$. Volume offset between the P-V curves remains constant. The mass ratio between Nb and $NbH_{0.5}$ as given by phase analysis amounts to ∼70/30%. Some irregular variation at different pressures can be explained by the preferred orientation as well as variations in grain size. In our experiment, we did not observe the bcc to body-centered-tetragonal (bct) phase transition at ∼30 GPa as reported previously for $NbH_{0.75}$ [37]. At 97 GPa, a third set of bcc peaks appears at yet lower angles like in our first run, but more pronounced. It points to another hydride phase with higher hydrogen content which coexists with $NbH_{0.5}$. We therefore suggest that spinodal decomposition takes place at these pressures. Hydrogen concentration in the noncoherent $\alpha$ phase is $x = 1.13$. The mass ratio between the phases $Nb/NbH_{0.5}/NbH_{1.13}$ at 110 GPa appears as ∼75/20/5%.

### B. Effect of laser heating

As the room-temperature runs pointed to slow kinetics of hydrogen dissolution, the necessary laser heating was applied to facilitate it. For the third run, cell 1 with flat anvils and cell 2 with beveled tips were loaded with the samples again. Cell 1 was compressed to 22 GPa, then half of the Nb foil was heated with the laser, and the other half was left as a reference. The beveled-anvil cell 2 was compressed to ∼50 GPa. The whole foil was heated (Fig. S3 in the Supplemental Material [36]), and the pressure decreased to 46 GPa. Temperature was visually estimated to be above 1500 K from the brightness and color with previous experience. Further compression and the XRD measurements were performed at room temperature after several days. The samples were scanned across the x-ray beam, and the spot to be probed was chosen so that no signal from the gasket was seen, yet cell 1 was positioned to maximize the number of peaks observed from the sample that corresponds to the border between the heated part and the rest. A summary of the diffraction patterns observed is presented in Fig. 1. At pressures from 22 to 35 GPa, all peaks were split except the reference sample, and two fcc phases were observed. The splitting increased with compression. At 39 GPa, the splitting disappeared, and a jump in the peak positions towards higher-angle values occurred indicating a phase transition. At pressures between 42 and 51 GPa, the diffraction profiles do not match any simple structure, even though a number of possibilities including preferred orientation, influence of grain size, and the predicted structure [18] were examined. In the end, the structure was identified as an hcp phase with stacking faults where the BCB-CACBABCBC stacking sequence fits best to the diffraction patterns. At 46 GPa, after laser heating, the sample in cell 2 appeared as a mixture of two phases with the hcp and the dhcp lattices (Fig. S4 in the Supplemental Material [36]). Under further compression, a third phase with cubic symmetry appeared at 56 GPa, most likely $NbH_3$ with a distorted bcc lattice ($I$-43$d$; hereafter denoted as $\delta$ phase) [18]. Above 56 GPa, only dhcp and $\delta$ phases were observed with the fractional increasing of the $\delta$ phase under pressure. The representative plots with the calculated versus experimental diffraction profiles are given in Fig. 2, which illustrates the reliability of the structure models.

It is hard to see hydrogen in the XRD experiments due to its much lower electron density against the metal, so the

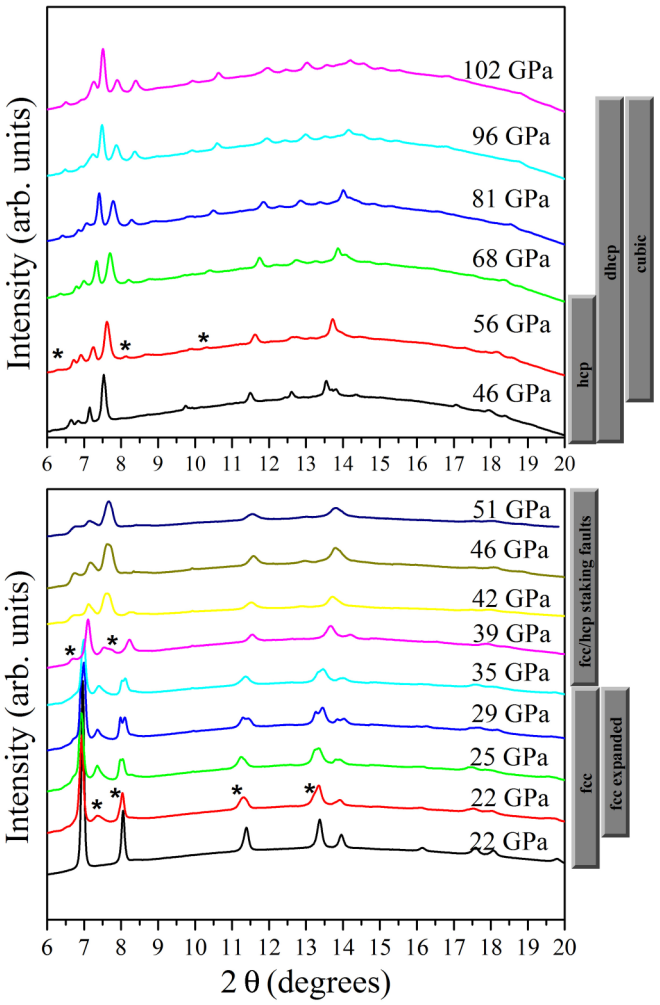


FIG. 1. ($\lambda = 0.308245$ Å) Diffraction patterns of the samples after heating under different pressure in (down) cell 1 and (up) cell 2. The downmost black pattern at 22 GPa is from the indirectly heated sample. The asterisks denote the new peaks of $NbH_x$.

immediate conclusion can be drawn from the structural analysis, which is related to the Nb sublattice only. We observed the formation of the predicted $\delta$-$NbH_3$ at high pressure. Also, several other phases appeared at lower pressures which were not expected theoretically. One of these phases having an fcc lattice could be identified as $\gamma$-$NbH_2$. But the appearance of the second fcc lattice with a different lattice parameter remains unclear. However, the formation of $NbH_3$ with fcc lattice is not excluded since it is enthalpically competitive with respect to the others. We further explored the observed phases by examining the hydrogen positions, hydrogen content, and their stability with respect to each other using the P-V data obtained and employing numerical DFT-based simulations.

## V. DISCUSSION

In order to facilitate the following discussions, some crystal structures of $NbH_x$ are shown in Fig. 3. Here, Nb forms metal sublattices, and all hydrogen atoms occupy T or octahedral (O) sites at different conditions.

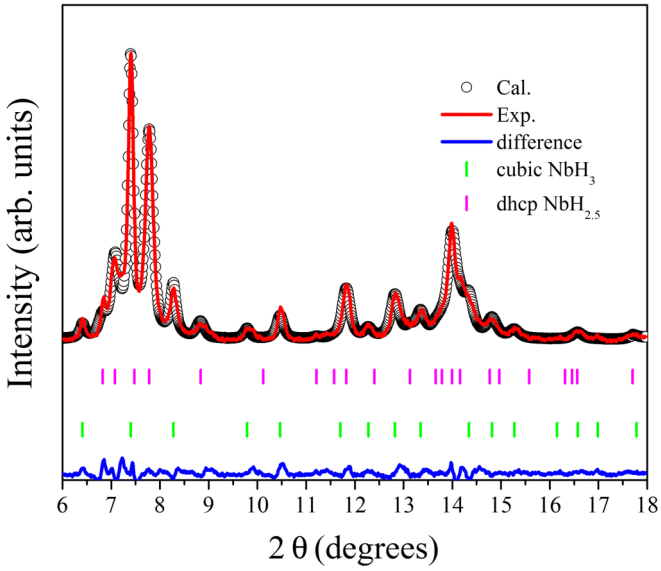


FIG. 2. The diffraction profile of mixed $NbH_{2.5}$ and $NbH_3$ at 81 GPa. The black open circles and red solid line represent the Rietveld fits and observed data, respectively, and the blue solid line is the residual intensity.

### A. EOS and hydrogen content

We used DFT calculations to locate the hydrogen positions inside the lattices and to obtain their EOSs for those structures which match the diffraction patterns observed. This enabled us to estimate the hydrogen content and locate hydrogen positions. For $\delta$-$NbH_3$, we used structural data from theory [18]. In order to calculate the EOS, hydrogen was placed into the interstitial sites of the close-packed lattices, and all atoms, as well as the unit cell volumes, were allowed to relax until the target pressure was achieved while the lattice structure remained fixed. Our calculations reproduced the experimental EOS for Nb, ambient-pressure volume of $\gamma$-$NbH_2$, and the EOS for $H_2$ well. This gave us grounds to rely on the EOS calculations for other compositions. We found that, after relaxation, in all cases, hydrogen remained in the interstitial sites as intuitively expected, due to the constraints imposed on hydrogen by the metal lattice.

In order to estimate the hydrogen content in our samples, first we examined the volumetric effect of hydrogen embedded in the Nb lattice. In Fig. S5 of the Supplemental Material [36], experimental P-V data for Nb [38] and bcc $NbH_x$ are plotted with the calculated EOSs for $NbH_2$ and $NbH_3$. For the bcc phase, our data provide further confirmation for the known fact for hydrogen being incompressible in Nb matrix. However, it is important to note that, by only comparing the P-V curves, it is impossible to distinguish between compressible hydrogen and the combined effect of the hydrogen volume reduction plus increase of hydrogen concentration with pressure. Our data coincide with those obtained with no hydrogen excess [37,39], so hydrogen in bcc $NbH_{x<1}$ appears truly incompressible. However, the behavior is not obvious for other lattices with higher hydrogen content. Therefore, we examined it by calculating the EOS for stoichiometric $NbH_2$ and $NbH_3$. Despite noticeable variations in the EOS for $NbH_2$, depending on the metal sublattice, it is

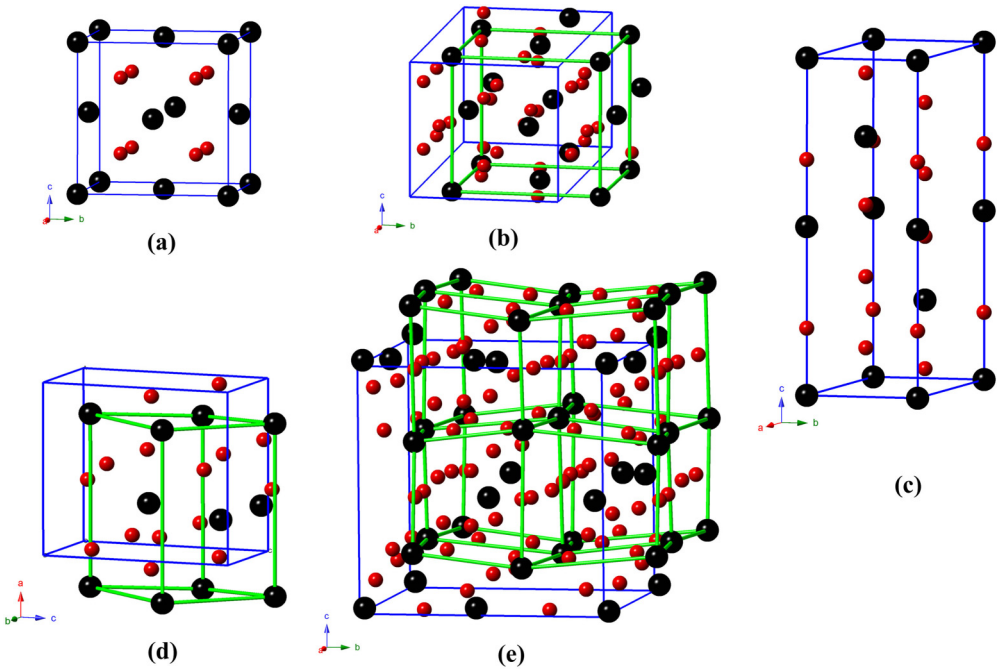


FIG. 3. The structures of (a) $NbH_2$ ($Fm$-$3m$) at 20 GPa, (b) $NbH_{2.5}$ ($Ibam$) at 20 GPa, (c) $NbH_{2.5}$ ($P6_3mc$) at 80 GPa, (d) $NbH_2$ ($Pnma$) at 50 GPa, and (e) $NbH_3$ ($I$-$43d$) at 80 GPa. Large and small spheres represent Nb and H atoms, respectively. The green cells represent the niobium sublattice.

evident that the third additional hydrogen atom results in lattice expansion as intuitively expected, although the amount of the expansion is less than that of the first and second atoms. A first approximation amounts to $\sim 1.4\,\text{Å}^3$/H atom with hydrogen being hardly compressible.

In Fig. 4, the experimental P-V points of the third run are plotted together with the calculated EOSs. The data from the higher-angle set of the fcc peaks agrees well with the calculated EOS for $\gamma$-$NbH_2$. This also allows us to conclude that the composition of stoichiometric $NbH_2$ remains constant

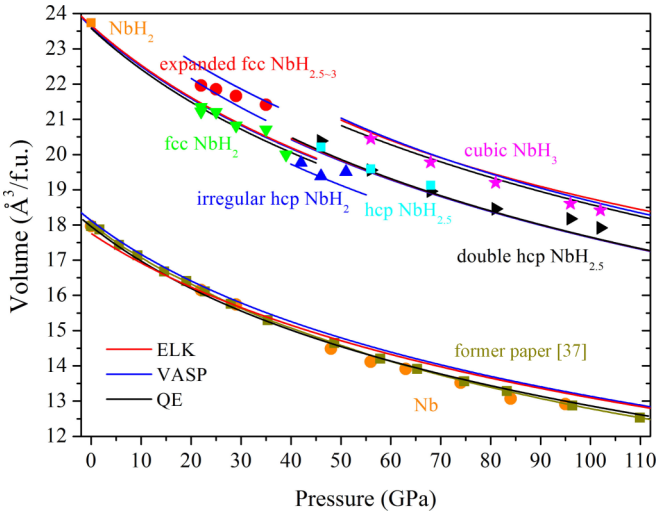


FIG. 4. Volumes as a function of pressure for the different $NbH_x$ phases, including a comparison of the element Nb with the former experimental paper [37]. The solid lines and symbols represent the simulations and experimental data, respectively.

under compression. The P-V points originating from the low-angle set of the fcc peaks are located between the calculated $CaF_2$-type $NbH_2$ and $BiF_3$-type $NbH_3$ curves. Assuming that the lattice expansion is proportional to the concentration of the third hydrogen atom, the total concentration can be estimated as varying from 2.5 at 22 GPa to 3 at 35 GPa. From 56 to 102 GPa, the experimental points for the cubic phase are close to the theoretical curve for $\delta$-$NbH_3$. The fact that the theoretical curve is slightly higher may indicate either a systematic error in the DFT calculations or that the actual hydrogen content is slightly less than three, just like what was observed in the Ir-H [21] and Fe-H [22] systems. The composition of the hcp and the dhcp phases appearing after heating at 46 GPa (cell 2) can be estimated as $NbH_{2.5}$. Interestingly, the experimental points which were identified as belonging to the dhcp lattice at pressures from 46 to 102 GPa agree fairly well with the calculated phase $NbH_{2.5}$ with $P6_3mc$ space group, where no disorder in the hydrogen subsystem is assumed. This gives additional confirmation for the composition.

### B. Phase transformations: Enthalpy analysis

The overall behavior of the sample under laser heating and compression is as follows. At 22 GPa, heating resulted in the formation of $\gamma$-$NbH_2$ as well as $NbH_{2.5}$ with the fcc lattice. Under further compression at room temperature, the $NbH_{2.5}$ hydrogen concentration increased up to $\sim$3 at 35 GPa. Between 35 and 39 GPa, structural instability appeared due to a first-order phase transition when the metal sublattice changed from fcc to hcp, and even the hcp phase is enthalpically unstable compared with the $Pnma$ phase in our DFT calculation (Fig. 5). Furthermore, the instability triggered a change in fcc $NbH_3$, losing a portion of hydrogen. As a result, a hexagonal

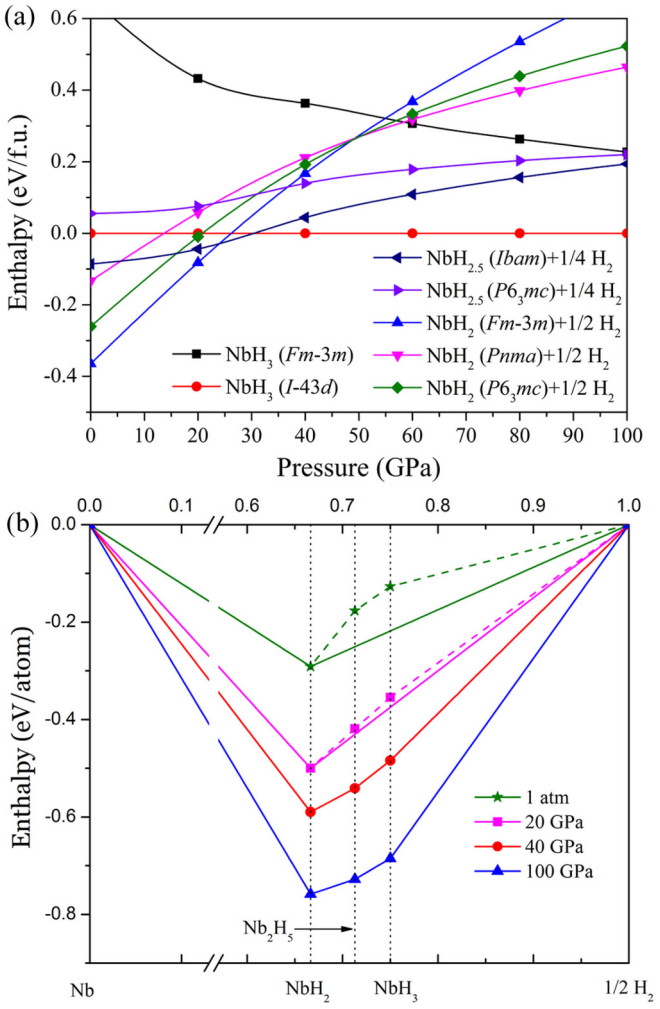


FIG. 5. (a) Enthalpy curves for various structures as a function of pressure. (b) Ground-state and static enthalpy of formation per atom of the $Nb_{1-x}H_x$ phases with respect to their separated counterparts; the hydrogen molar content ($x = 0$ corresponds to pure niobium; $x = 1$ to pure hydrogen) for the ground state and $P = 1$ atm, 20, 40, 100 GPa. Only related stoichiometries are plotted; others are not considered here. The symbols on the solid lines denote that the hydrides are stable at the corresponding pressures, while those on the dashed lines represent that the hydrides are unstable with respect to their decomposition into hydrogen and other hydride or niobium.

$NbH_2$ with irregular or long-period stacking sequence formed. Apparently, such a lattice is formed due to slow kinetics which results in an incomplete phase transition. When the sample was heated at 46 GPa, two new distinct phases appeared: hcp and dhcp. Apparently, annealing takes place here. Under compression, the sequence of phases appeared first as fcc, then hcp, dhcp, and lastly distorted bcc. The large overlapped ranges of pressure, where these phases were observed, point to slow kinetics.

Now, we examine whether this behavior can be rationalized in terms of enthalpic stability. Since we do not have an adequate model for $NbH_x$ with a fractional $x$ which would account for the possible disorder in the hydrogen subsystem, we examined three extreme cases with $x = 2$, 2.5, and 3. When we applied structural search algorithms to the composition with $x = 2.5$, we found that at least 50 structures shared nearly the same (within ~0.01 eV) enthalpy $H_{\min}$ characteristic, which is lower than their close-packed structures at all pressures. The *Ibam* phase is shown as representative one containing a distorted fcc lattice. Figure 5 shows that there may be a transition from the $\gamma$ phase to the *Pnma* phase in $NbH_2$, even though we observed hcp $NbH_2$ experimentally. The convex shows that $NbH_{2.5}$ and $NbH_3$ appear to be more stable at high pressures. Therefore, a modification of the stability relationships between these structures occurs as more hydrogen is added to the system. In principle, such behavior explains the observed phase sequence assuming appropriate variations in hydrogen concentration under pressure. Nevertheless, even lower enthalpy is characteristic of the $\delta$ phase. When comparing it with $NbH_2$ or $NbH_{2.5}$ plus hydrogen, it turns out that this phase becomes stable at ~27 GPa. In other words, $\delta$ phase could form directly from fcc $NbH_{2-2.5}$, by skipping the hcp and the dhcp phases, as it occurs in the Ir-H system [21]. However, this contradicts what we observed experimentally, and some metastable phases appear. Interestingly, similar behavior is also observed in the Fe-H system, where the formation of cubic $FeH_3$ at 87 GPa is preceded by the formation of tetragonal $FeH_{\sim 2}$ at 67 GPa, which is also enthalpically unstable with respect to the cubic one [22]. A possible explanation is that enthalpy analysis implies zero temperature, whereas full Gibbs free energy should be considered at finite temperatures.

### C. Finite temperatures

Our enthalpy calculations results suggest that $BiF_3$-type $NbH_3$ should never form because its enthalpy is always higher than the other phases at corresponding pressure. At 20 GPa, the enthalpy difference between fcc $NbH_3$ and fcc $NbH_2 + 1/2\,H_2$ amounts to 0.73 eV/f.u. (Fig. 5). This value sets the scale of Gibbs free energy, which is necessary to embed the third hydrogen atom in the metal matrix. The thermal energy associated with laser heating in our experiment amounts to $k_B T \sim 0.19$ eV/atom or 0.76 eV/f.u. This estimate demonstrates that heating to ~1500 K can supply deficient energy for overcoming the kinetic barrier and forming fcc $NbH_3$. We therefore suggest that fcc $NbH_{2.5-3}$ ($\gamma'$ phase) is the high-temperature phase which is stable from 22 to 35 GPa. In our experiment, the $\gamma'$ phase formed in the part of the sample which was directly heated by laser. The $\gamma$-$NbH_2$ was formed in the adjacent part which was heated by thermal conductivity and therefore experienced a somewhat lower temperature.

In principle, a similar consideration may apply when hcp and dhcp $NbH_{2.5}$ are formed at 46 GPa. Here, thermal energy well exceeds the enthalpy difference between the hcp/dhcp phase and the *Ibam* phase (Fig. S6 in the Supplemental Material [36]). However, the phase transition from the fcc to the hcp/dhcp phases appears to be pressure induced at room temperature. Therefore, the role of heating is simply to perform annealing to complete the transition. Thus, the mechanism which stabilizes these structures remains questionable. A possible cause is the disorder in the hydrogen subsystem which increases the entropy term in the Gibbs function, but evaluation of configurational entropy is out of our current reach. Other possibilities could be local stress and anharmonic effects, as suggested for $IrH_3$ [21].

### D. High concentrations versus low concentrations: States of hydrogen in Nb

When a single hydrogen atom is placed into the interstitial site of the metal lattice, the surrounding metal atoms are displaced outwards, and hydrogen adopts the so-called self-trapped state where the lowering of the hydrogen embedding energy due to local lattice expansion is balanced by an increase of elastic energy [3]. A number of experimental phenomena indicate that, when a hydrogen atom occupies an interstitial site, several neighboring interstices get blocked with blocking radius extended over three or four coordination spheres [2]. The minimum possible distance between the hydrogen atoms appears to be around 0.7–0.8 $a$ ($a$ is the lattice constant). In the self-trapped state, proton wave functions are localized within $\sim 1/4\,a$, so it is argued that hydrogen interacts essentially with the neighboring metal atoms, while a long-range interaction between the hydrogen atoms occurs indirectly via the strain field of metal lattice [3]. A highly localized proton wave function underlines the empirical finding that, in many cases, hydrogen can be treated as a hard sphere with radius of $r_H \approx 0.56$ Å [2]. In particular, the hard sphere model is consistent with the empirical observation that the type of the hydrogen-occupied interstices depends on the size of the host metal atom: in the hosts where the atoms are smaller than some critical value, hydrogen occupies O sites, otherwise the T ones are occupied [23]. Overlapping of the strain fields around the occupied sites results in uniform host lattice expansion which amounts to the universal value $V_H = 2.9$ Å$^3$/H atom mentioned above.

In the close-packed lattices, there are three interstitial sites per metal atom in total. So at hydrogen concentrations with $x > 2$ most of neighboring interstices are filled out. This means that blocking effects cannot hold in the high-concentration phases, and the closest distance between hydrogen atoms appears as 0.43 $a$ (the distance between O and T sites in the fcc lattice). This is nearly twice as small as the low-concentration phases, so one can expect an increase of direct H-H interactions. Also, the ratio between the number of interstices available and the number of hydrogen atoms is drastically decreased in the high-concentration phases (in the bcc lattice, there are six T and three O interstices per metal atom). Subsequently, the ordering conditions in the hydrogen subsystem, and therefore the way the configurational entropy is calculated [40], should also experience major modifications. Its influence on other properties, for example, hydrogen mobility which at low concentrations is determined by tunneling over the interstices, remains an intriguing problem to study.

Considering the lattice expansion due to hydrogen dissolution, we noticed that it amounts to $V_H = 2.49$ Å$^3$/H atom for $\gamma$-$NbH_2$ when the calculated fcc Nb lattice was taken as the reference structure, which is significantly smaller than for $x < 1$. In the $NbH_3$ phase, lattice expansion is further reduced to $V_H = 2.0$ Å$^3$/H atom. It is natural to associate this remarkable reduction of lattice expansion as a function of concentration with enhanced direct interactions between hydrogen atoms. When volume is viewed as a function of pressure, we notice that partial hydrogen volume in the high-concentration phases is somewhat reduced under compression compared with "totally" incompressible hydrogen at low concentrations. Although this effect is not well pronounced enough to make definitive conclusions, it is consistent with the suggestion that such behavior results from increased density of states at the Fermi level [23].

Next, we consider the phase transition from the fcc phase to the hcp/dhcp phases. In $\gamma$-$NbH_2$, hydrogen is known to occupy T interstices, and on further saturation, the O interstices are occupied. On the other hand, when Nb atoms are arranged either in hcp or in dhcp lattices, the energy of the configuration where both H atoms occupy T interstices is significantly higher than that occupying O and T. In other words, the phase transition in $NbH_2$ from the $\gamma$ phase to either of the hexagonal phases is associated with the migration of H atoms from the T interstices to the O ones. The T interstices become occupied when $x > 2$ because all the O interstices are filled out. In fact, such a transition was predicted on the basis of the site preference model. Indeed, the atom size of Nb ($V_{Nb} = 18$ Å$^3$/atom) corresponds to the border between the T and O site occupancy for the 4$d$ metals. Here, Mo, which is next to Nb in the periodic table, has smaller atoms ($V_{Mo} = 15.6$ Å$^3$/atom), and hydrogen occupies O interstices. Under compression, the atomic volume of Nb is reduced to $V_{Nb} = 15$ Å$^3$/atom at 39 GPa, so hydrogen should migrate from the T to the O interstices [23]. This is what was observed in $NbH_{0.75}$ at about 30 GPa [37] and also appears to be valid at high concentrations. Actually, in our experiment, we did not observe stoichiometric $NbH_2$ in the hcp/dhcp form. This seems to reflect the fact that the behavior of the hcp/dhcp phase is different from the fcc one: if the T interstices are occupied on top of the O sites, high temperature is not required to dissolve hydrogen above $x = 2$.

## VI. CONCLUSIONS

Hydrogen concentrations as high as $x \sim 2.5-3$ can be reached in a megabar pressure range when sufficient high temperature is applied. In particular, we observed stoichiometric $\delta$-$NbH_3$ with a distorted bcc lattice. However, the phase diagram is more complicated than expected from our enthalpy considerations. Three more phases appear where Nb atoms are arranged in the closed packings. These phases appear to be more stable at moderate pressures and room temperature, so the transition into $\delta$-$NbH_3$ shifts from the predicted 33 to 56 GPa. All types of close-packed lattices were observed. The appearance of the phases with close-packed Nb sublattices cannot be explained in terms of enthalpic stability, except $\gamma$-$NbH_2$. Heating is crucial, and temperature appears to have a double role: when it reached a certain region in the phase diagram, $\gamma'$-$NbH_{2.5}$ appeared at 22 GPa, while the phase transition from fcc to the hcp/dhcp $NbH_{2.5}$ was pressure induced and temperature annealed the sample. Across the fcc to hcp/dhcp transition, the hydrogen-occupied site preference changes, so that the O interstices are occupied first before the T interstices. The compressional behavior of the hydride appears identical to the behavior of the host metal with hydrogen and is nearly incompressible over the whole range studied.

The structural and compressional behaviors of the Nb-H system appear different from the Ir-H and Fe-H systems. The compressibility of both Ir-H and Fe-H hydrogen-rich alloys

behaves similarly, and each of them substantially differs from the corresponding host metal. This implies that the hydrogen subsystem determines such behavior. On the contrary, in the Nb-H system, at similar hydrogen concentrations, both the hydrogen site preference and compressibility appeared identical to the characteristics of "traditional" hydrides with a low hydrogen content. Nevertheless, it is remarkable that the magnitude of the lattice expansion due to hydrogen dissolution appears as a decreasing function of the number of dissolved hydrogen atoms. That points to substantial modification of interatomic bonding towards enhancing the H-H interaction as the hydrogen concentration is increased. Thus, the hydrogen-determined behavior seems to emerge at the concentrations reached. The impact of these changes on other alloy properties is still to be studied. Also, the mechanisms which stabilize the close-packed lattices and call into question the degree of disorder in the hydrogen subsystem are still unresolved. The hydrogen mobility in these alloys is also of particular interest (at low concentrations, it is very high as determined by tunneling over interstices).

Our results demonstrate the important role of temperature which, when high enough, enables us to uncover phases with high hydrogen concentrations at moderate pressures. Nevertheless, the complex phase diagram combined with slow kinetics makes experimental results highly sensitive to the thermodynamic path maintained in the experiment. This may make this system difficult to study in terms of material science because experimental results may appear inconsistent from one run to another.

## ACKNOWLEDGMENTS

We thank to I. Troyan for his help with the DAC experiments. We also thank A. Kleppe for her help at beamline I15 of Diamond Light Source, as well as the staff of beamline P02.2. at PETRA III Synchrotron Source. Parts of this research were carried out at the light source PETRAIII at Deutsches Elektronen-Synchrotron (DESY), a member of the Helmholtz Association (HGF). The authors acknowledge funding support from the National Natural Science Foundation of China under Grants No. 11534003, No. 11604314, and No. 11604290, the National Key Research and Development Program of China (under Grant No. 2016YFB0201200), 2012 Changjiang Scholar of Ministry of Education, and Science Challenge Project (under Grant No. JCKY2016212A501). The authors also would like to thank the China Scholarship Council under Award No. 201206170130 and Russian National Research Centre Kurchatov Institute for their partial support of this paper. Work at Max Planck Institute for Chemistry was supported by the European Research Council 2010-Advanced Grant 267777. Work at Carnegie was supported by Energy Frontier Research in Extreme Environments Center (EFree), an Energy Frontier Research Center funded by the Department of Energy (DOE), Office of Science, Basic Energy Sciences under Award No. DE-SC-0001057. The infrastructure and facilities used at Carnegie were supported by National Nuclear Security Administration (NNSA) Grant No. DE-NA-0002006, Carnegie/Department of Energy Alliance Center (CDAC).

[1] G. Alefeld and J. Völkl, *Hydrogen in Metals* (Springer-Verlag, Berlin, 1978).
[2] V. A. Somenkov and S. S. Shil'stein, Prog. Mater. Sci. **24**, 267 (1980).
[3] Y. Fukai, *The Metal-Hydrogen System* (Springer-Verlag, Berlin, 2005).
[4] L. Schlapbach and A. Züttel, Nature **414**, 353 (2001).
[5] S. Niaz, T. Manzoor, and A. H. Pandith, Renew. Sustain. Energy Rev. **50**, 457 (2015).
[6] N. W. Ashcroft, Phys. Rev. Lett. **92**, 187002 (2004).
[7] A. P. Drozdov, M. I. Eremets, I. A. Troyan, V. Ksenofontov, and S. I. Shylin, Nature **525**, 73 (2015).
[8] Y. Li, J. Hao, H. Liu, Y. Li, and Y. Ma, J. Chem. Phys. **140**, 174712 (2014).
[9] N. Ashcroft, Phys. Rev. Lett. **21**, 1748 (1968).
[10] A. E. Carlsson and N. W. Ashcroft, Phys. Rev. Lett. **50**, 1305 (1983).
[11] E. Zurek, R. Hoffmann, N. W. Ashcroft, A. R. Oganov, and A. O. Lyakhov, Proc. Natl. Acad. Sci. USA **106**, 17640 (2009).
[12] P. Baettig and E. Zurek, Phys. Rev. Lett. **106**, 237002 (2011).
[13] H. Wang, J. S. Tse, K. Tanaka, T. Iitaka, and Y. Ma, Proc. Natl. Acad. Sci. USA **109**, 6463 (2012).
[14] Y. Li, J. Hao, H. Liu, J. S. Tse, Y. Wang, and Y. Ma, Sci. Rep. **5**, 9948 (2015).
[15] X. Feng, J. Zhang, G. Gao, H. Liu, and H. Wang, RSC Adv. **5**, 59292 (2015).
[16] Evgenii G Maksimov and O. A. Pankratov, Sov. Phys. Usp. **18**, 481 (1975).
[17] P. Zaleski-Ejgierd, V. Labet, T. A. Strobel, R. Hoffmann, and N. W. Ashcroft, J. Phys.: Condens. Matter **24**, 155701 (2012).
[18] G. Gao, R. Hoffmann, N. W. Ashcroft, H. Liu, A. Bergara, and Y. Ma, Phys. Rev. B **88**, 184104 (2013).
[19] B. Li, Y. Ding, D. Y. Kim, R. Ahuja, G. Zou, and H.-K. Mao, Proc. Natl. Acad. Sci. USA **108**, 18618 (2011).
[20] T. Scheler, F. Peng, C. L. Guillaume, R. T. Howie, Y. Ma, and E. Gregoryanz, Phys. Rev. B **87**, 184117 (2013).
[21] T. Scheler, M. Marqués, Z. Konôpková, C. L. Guillaume, R. T. Howie, and E. Gregoryanz, Phys. Rev. Lett. **111**, 215503 (2013).
[22] C. M. Pépin, A. Dewaele, G. Geneste, P. Loubeyre, and M. Mezouar, Phys. Rev. Lett. **113**, 265504 (2014).
[23] V. A. Somenkov, V. P. Glazkov, A. V. Irodova, and S. S. Shilstein, J. Less-Common Met. **129**, 171 (1987).
[24] J. J. Reilly and R. H. Wiswall, Inorg. Chem. **9**, 1678 (1970).
[25] Y. Akahama and H. Kawamura, J. Phys.: Conf. Ser. **215**, 012195 (2010).
[26] A. F. Goncharov, E. Gregoryanz, R. J. Hemley, and H. Mao, Proc. Natl. Acad. Sci. USA **98**, 14234 (2001).
[27] M. A. Pick, J. W. Davenport, M. Strongin, and G. J. Dienes, Phys. Rev. Lett. **43**, 286 (1979).
[28] J. Rodrigues-Carvajal, Comm. Powder Diffrac. (IUCr) Newslett. **26**, 12 (2001).

[29] G. Kresse and J. Furthmüller, Phys. Rev. B **54**, 11169 (1996).
[30] P. Giannozzi, S. Baroni, N. Bonini, M. Calandra, R. Car, C. Cavazzoni, D. Ceresoli, G. L. Chiarotti, M. Cococcioni, I. Dabo, A. Dal Corso, S. de Gironcoli, S. Fabris, G. Fratesi, R. Gebauer, U. Gerstmann, C. Gougoussis, A. Kokalj, M. Lazzeri, L. Martin-Samos *et al.*, J. Phys.: Condens. Matter **21**, 395502 (2009).
[31] The Elk Full-Potential Linearized Augmented Plane Wave, Available at http://elk.sorceforge.net.
[32] Y. Wang, J. Lv, L. Zhu, and Y. Ma, Phys. Rev. B **82**, 094116 (2010).
[33] Y. Wang, J. Lv, L. Zhu, and Y. Ma, Comput. Phys. Commun. **183**, 2063 (2012).
[34] L. Kleinman and D. M. Bylander, Phys. Rev. Lett. **48**, 1425 (1982).
[35] A. Togo and I. Tanaka, Scr. Mater. **108**, 1 (2015).
[36] See Supplemental Material at http://link.aps.org/supplemental/10.1103/PhysRevB.95.104110 for the other XRD patterns, sample photographs, refinement, DFT calculations, and crystal structure details of $NbH_x$.
[37] A. Fukizawa and Y. Fukai, J. Phys. Soc. Jpn. **52**, 2102 (1983).
[38] T. Kenichi and A. K. Singh, Phys. Rev. B **73**, 224119 (2006).
[39] H. Taguchi, Y. Fukai, T. Atou, K. Fukuoka, and Y. Syono, Phys. Rev. B **49**, 3025 (1994).
[40] J. Garcés, Appl. Phys. Lett. **96**, 161904 (2010).